文章编号：1001-9014(2020)06-0709-09

DOI:10.11972/j.issn.1001-9014.2020.06.008

Millimeter wave security imaging based on single-channel MIMO radar

MA Zhao-Hui[1], WANG Jing-Yang[2], JING Han-Dan[1], LIU Fan[3*], HU Wei-Dong[1], LYU Xin[1]

(1. Beijing Key Laboratory of Millimeter Wave and Terahertz Technology, School of Information and Electronics, Beijing Institute of Technology, Beijing 100081, China;
2. Department of Electronic Engineering, Tsinghua University, Beijing 100084, China;
3. Department of Electronic and Electrical Engineering, University College London, London WC1E 7JE, U. K.)

Abstract: Millimeter wave (mmW) multiple-input multiple-output (MIMO) radar is state-of-the-art technique for security imaging. However, the exploitation of large number of transmit/receive channels leads to much higher cost and complexity for the MIMO radar than that of the single-channel radars. Aiming for developing the low-cost and low-complexity mmW MIMO security imaging radar, dual-code-division-multiplex (dual-CDM) technique has been proposed in this paper. It is worth noting that the proposed method can realize the similar imaging performance with the traditional multi-channel MIMO radar by a single transmit /receive channel, which is of great significance for the development and application in the area of security imaging. Moreover, the de-multiplex code, which can attain the maximum code diversity gain against the interference, is designed based on mismatched filter theory. Finally, both the numerical and the experimental results are provided to verify the correctness and the validity of the proposed methods, which shows that quite a satisfactory imaging performance is achieved.

Key words: millimeter wave (mmW) imaging, multiple-input multiple-output (MIMO), single-channel, code-division-multiplex (CDM), mismatched filter

PACS: : 84. 40. Ua

基于单通道MIMO雷达的毫米波安检成像

马朝辉[1], 王晶阳[2], 敬汉丹[1], 刘 凡[3*], 胡伟东[1], 吕 昕[1]

(1. 北京理工大学 信息与电子学院 毫米波与太赫兹技术北京市重点实验室,北京 100081;
2. 清华大学 电子工程系,北京 100084;
3. 伦敦大学学院 电子与电气工程系,英国 伦敦 WC1E 7JE)

摘要:毫米波多入多出(MIMO)雷达是一种前沿的安检成像技术。然而,由于采用了大量的发射/接收通道,MIMO雷达的成本和复杂度大大高于传统的单通道雷达。为了研制低成本、低复杂度的毫米波MIMO安检成像雷达,引入了双重码分复用技术。该方法可通过单发射/接收通道实现与传统多通道MIMO雷达相似的成像性能,对安检成像领域的发展和应用具有重要意义。此外,设计了基于失配滤波器理论的解复用码,其可在干扰条件下实现最大码分集增益。进行了仿真与实验以验证所提出方法的正确性与有效性,得到了满意的结果。

关 键 词:毫米波成像;多入多出(multiple-input multiple-output ,MIMO);单通道;码分复用;失配滤波器

中图分类号:TN957.7 **文献标识码**:A

Introduction

Millimeter wave (mmW) has the characteristics of transparency to fiber, non-ionization to biological tissue, and relatively higher resolution compared with micro-

Received date: 2019- 12- 15, **revised date**: 2020- 04- 17 **收稿日期**:2019- 12- 15,**修回日期**:2020- 04- 17

Foundation items: Supported by National Natural Science Foundation of China (61901040, 61527805), the Joint Research Fund in Astronomy (U1631123) under a cooperative agreement between the National Natural Science Foundation of China and the Chinese Academy of Sciences.

Biography: MA Zhao-Hui (1989-), male, Henan China, Ph. D. Research area involves MIMO radar imaging and optimization technique. E-mail: mzh_19890822@bit. edu. cn

[*] **Corresponding author**: fan. liu@ucl. ac. uk

wave, which makes mmW a promising frequency band for security imaging [1-9]. Among all the mmW imaging technologies, multiple-input multiple-output (MIMO) radar that takes advantage of the multiple-antenna structure is an emerging approach. By exploiting the orthogonal diversity of the probing signals, a MIMO radar system that consists of M transmit elements (TEs) and N receive elements (REs) can equivalently form MN individual observation channels, which is typically much larger than $M + N$. This facilitates the acquisition of a large amount of observation data by relying on small-scale arrays. However, this requires the deployment of $M + N$ RF channels in the traditional MIMO radar system, which inevitably leads to increasing cost, size, heat dissipation and power consumption.

To tackle the above issues, the sparse array theory has been widely studied as a promising solution for system design [10-14]. Although the number of elements can be reduced to a certain extent, the performance will deteriorate with the decrease of the number of the observation channels as well. In Ref. 15, a low latency digital beamforming radar using aperture coding is proposed, where a single channel phased array radar is achieved for the car application. Pioneered by Ref. 16, a code-division-multiplex (CDM) based spread spectrum digital beamforming (SSDBF) technique has been proposed, which enables the phased array radar to work with just one RF channel module. To realize perfect signal recovery in SSDBF, the truly shift orthogonal code (TSOC) is designed as the de-multiplex code. Inspired by this work, [17-19] study the application of SSDBF in automotive radar, while [20-21] further investigate a software-defined phased array radar based on SSDBF. Moreover, hybrid analog-digital beamforming technique has been proposed for the massive MIMO system in 5G mmW applications [22], which is closely related to the MIMO radar technique proposed in this work. To the best of our knowledge, however, low-cost, and low-complexity designs for MIMO radar remain widely unexplored. Additionally, while the TSOC modified from m-sequence has a perfect-zero shift-phase correlation, it yields just one half of the code diversity gain compared to that of the original m-sequence.

Considering the above discussions, CDM is a promising technique for the low-cost and low-complexity radar, which is therefore exploited to develop the single-channel mmW MIMO security imaging radar system in this paper. To enhance the single-channel MIMO radar's performance, a de-multiplex code with the maximum code diversity gain as well as low shift-phase correlation is designed based on mismatched filter theory. Finally, simulation and experimental results are provided to verify the correctness and validity of the proposed methods.

1 Single-channel MIMO radar based on dual-CDM technique

1.1 Architecture of single-channel MIMO radar

Featured with the multi-antenna structure in both the transmit and receive array, the traditional MIMO radar usually calls for multiple channels containing full digital transceiver including up/down-converter, DAC/ADC, memory and digital interface. As shown in Fig. 1, a transmit/receive channel per antenna is essential to obtain all the individual observations, leading to a high cost and complexity of the radar system. For a MIMO radar with M TEs and N REs, M orthogonal signals should be generated and transmitted by M different transmit channels and antennas, respectively. Then the orthogonal signals will propagate over the space together, and the echo of every RE is a mixed signal containing all the transmitted signals. Although only N received signals are obtained in N receive channels, each of them can be separated into M components with digital signal processing method, due to the orthogonality of the transmitted signals. Therefore, M transmit channels and N receive counterparts are of the essence in the traditional MIMO radar system.

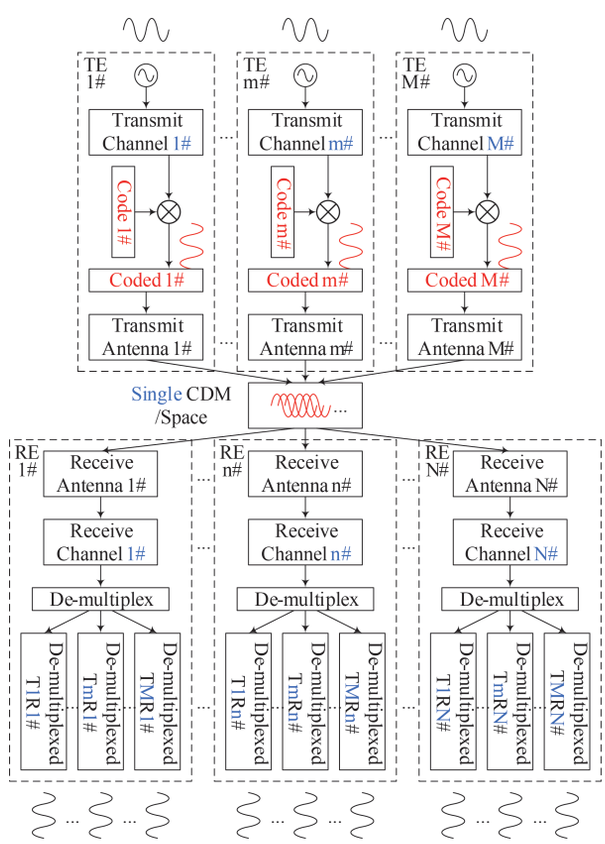

Fig. 1 Single-CDM process in traditional MIMO radar
图1 传统MIMO雷达中的单码分复用过程

It can be found that the number of channels can be reduced by the utilization of orthogonal signals, which are usually generated by the code-division-multiplex (CDM) technique. As shown in Fig. 2, to reduce the usage of transmit channels, a power divider can be employed before the CDM process. For further optimization of the number of the receive channels, another CDM process can be introduced as soon as the echoes incident on the REs. Then the N re-coded echoes can be mixed and processed together in a single receive channel, including

the down-convertor, ADC, memory and digital interface. It should be emphasized that a series of proper secondary CDM codes are of great significance to keep the orthogonality among all the *MN* individual observations. Therefore, combining the dual-CDM technique as well as the cheap and simple phase shifters, a MIMO radar front-end with a single transmit channel and a single receive counterpart can be realized, whose architecture can be designed as Fig. 3. The detailed process of the secondary CDM method will be discussed in the following section.

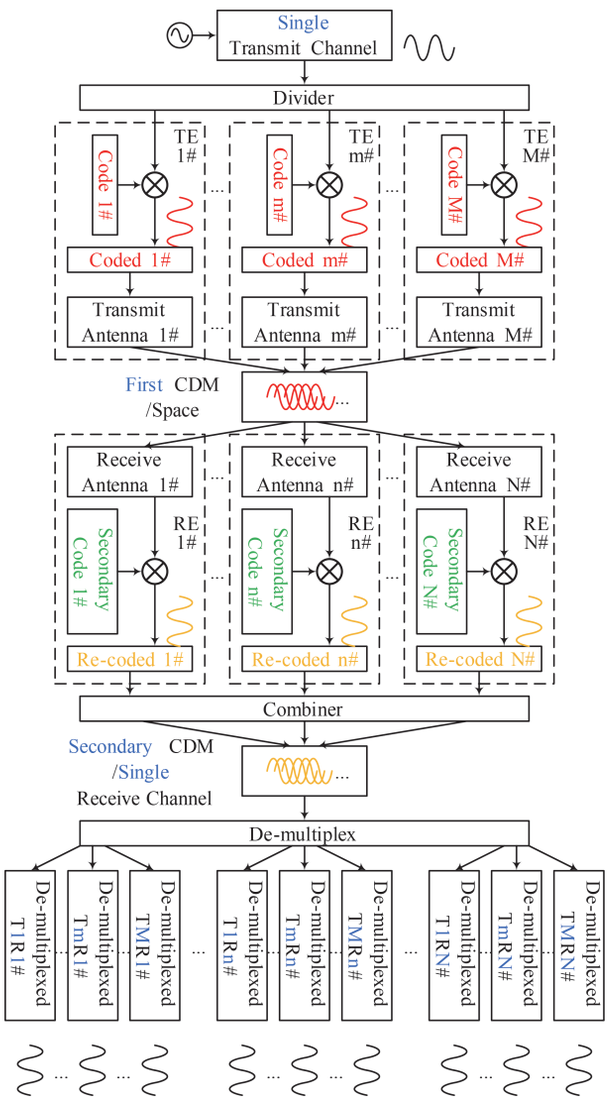

Fig. 2　Dual-CDM process in single-channel MIMO radar
图2　单通道MIMO雷达中的双重码分复用过程

1.2　Details of the secondary CDM process

As mentioned above, the secondary CDM is introduced to make it possible that all received signals occupy the single receive channel. Therefore, a key requirement for the single-channel MIMO radar is the separability of the *MN* signals from the different observation channels. In other words, these signals should also equivalently formulate the same *MN* observation channels to keep the radar's performance.

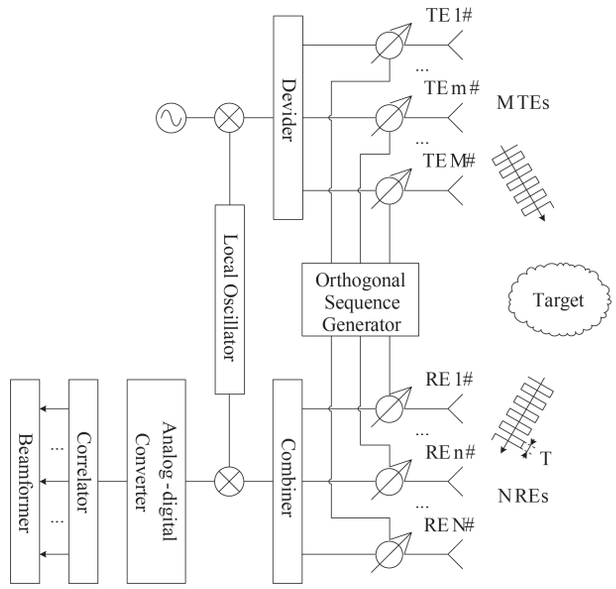

Fig. 3　Block diagram of the single-channel MIMO radar front-end
图3　单通道 MIMO 雷达前端系统框图

To our best knowledge, maximal length sequence, also named m-sequence, is the only binary sequence that has a shift-and-add property [23], which means the Hadamard product of two different m-sequences of one family generates a third m-sequence of this family. Meanwhile, it is worth highlighting that m-sequence is cyclic, which means a phase-shifted m-sequence also belongs to the same family. Based on this cyclic property, the index of an m-sequence is defined here for easy illustration in the following. Without loss of generality, we assign one of the sequences from a fixed length m-sequence family as the first sequence by default, and all the other sequences are ordered by their shift-phases. Table 1 shows the Hadamard product results generated by the p-th and the q-th sequence of a 15-length m-sequence family.

Based on the shift-and-add property and the cyclic property, the re-coded sequences in the aggregated signal to be de-multiplexed are controllable and predictable. Obviously, all the coded sequences used should be different from the others and all echoes should be received within one code chip time.

Let p_k be the k-th chip phase of the first sequence of a 15-length m-sequence family, T the code chip time, τ_{mn} the round-trip delay between the m-th TE and the n-th RE. Then following the rules above, Fig. 4 shows a detailed secondary CDM process of an exemplary 2×2 single-channel MIMO radar that utilizes a 15-length m-sequence family.

Before the analysis of Fig. 4, the time-code duality of the sequences should be clarified, which means each code chip of a sequence in practice has a duration time. In Fig. 4, the modulation waveforms in each code chip are omitted and just the code chips in time domain are remained. In the practical application, the re-coding signals of two sequences in the secondary CDM are usually

表1 长度为15的m序列Hadamard积结果表

Table 1 List of the Hadamard product results by 15-length m-sequences

q \ p	1	2	3	4	5	6	7	8	9	10	11	12	13	14	15
1	–	13	10	5	4	11	9	14	7	3	6	15	2	8	12
2	13	–	14	11	6	5	12	10	15	8	4	7	1	3	9
3	10	14	–	15	12	7	6	13	11	1	9	5	8	2	4
4	5	11	15	–	1	13	8	7	14	12	2	10	6	9	3
5	4	6	12	1	–	2	14	9	8	15	13	3	11	7	10
6	11	5	7	13	2	–	3	15	10	9	1	14	4	12	8
7	9	12	6	8	14	3	–	4	1	11	10	2	15	5	13
8	14	10	13	7	9	15	4	–	5	2	12	11	3	1	6
9	7	15	11	14	8	10	1	5	–	6	3	13	12	4	2
10	3	8	1	12	15	9	11	2	6	–	7	4	14	13	5
11	6	4	9	2	13	1	10	12	3	7	–	8	5	15	14
12	15	7	5	10	3	14	2	11	13	4	8	–	9	6	1
13	2	1	8	6	11	4	15	3	12	14	5	9	–	10	7
14	8	3	2	9	7	12	5	1	4	13	15	6	10	–	11
15	12	9	4	3	10	8	13	6	2	5	14	1	7	11	–

not strictly aligned in time domain due to the time delays. In this case, two sequences will be generated for one pair of TE and RE. It is obvious that the duration times of these two sequences are complementary to each other, which results in the alternant appearance of the chips of these two sequences. Therefore, two time axes $t_{m,n-1}$ and $t_{m,n-2}$ can be established to depict the two generated sequences of the m-th TE and the n-th RE, and the syntagmatic relation of t, $t_{m,n-1}$, $t_{m,n-2}$ and $\tau_{m,n}$ is embodied in the Fig. 4. In the example in Fig. 4, the two TEs are allocated with the 1-st and the 2-nd code sequences, and the two REs are allocated with the 3-rd and the 9-th counterparts. According to Table. 1, TE 1# and RE 1# generate the 10-th sequence on $t_{1,1-1}$ and the 5-th sequence on $t_{1,1-2}$, and all the other sequences' generation and relation can be analyzed likewise.

2 De-multiplex code design based on mismatched filter

2.1 Criterion of de-multiplex code design

After the dual-CDM process illustrated above, MN re-coded sequences are aggregated in the single receive channel for further process including down-conversion, sampling and so on. To recover the MN individual observations effectively, it is of great significance to separate these aggregated signals by proper de-multiplex method in digital domain. As mentioned above, the mixed MN re-coded sequences are orthogonal to each other, providing the foundation of de-multiplex process. Generally, the orthogonal signals will be separated by the correlation operation shown in Fig. 5.

As shown in Fig. 5, the expected signal can be accumulated effectively by a proper correlation kernel, while the unexpected counterparts, including the noise and the other signals, will be suppressed due to the incoherence. To achieve the best performance of the separation, a reasonable criterion should be studied. As the best-known method, the matched filter can achieve the maximum signal-to-noise ratio (SNR). Nevertheless, along with the noise, the interference is also quite an in-

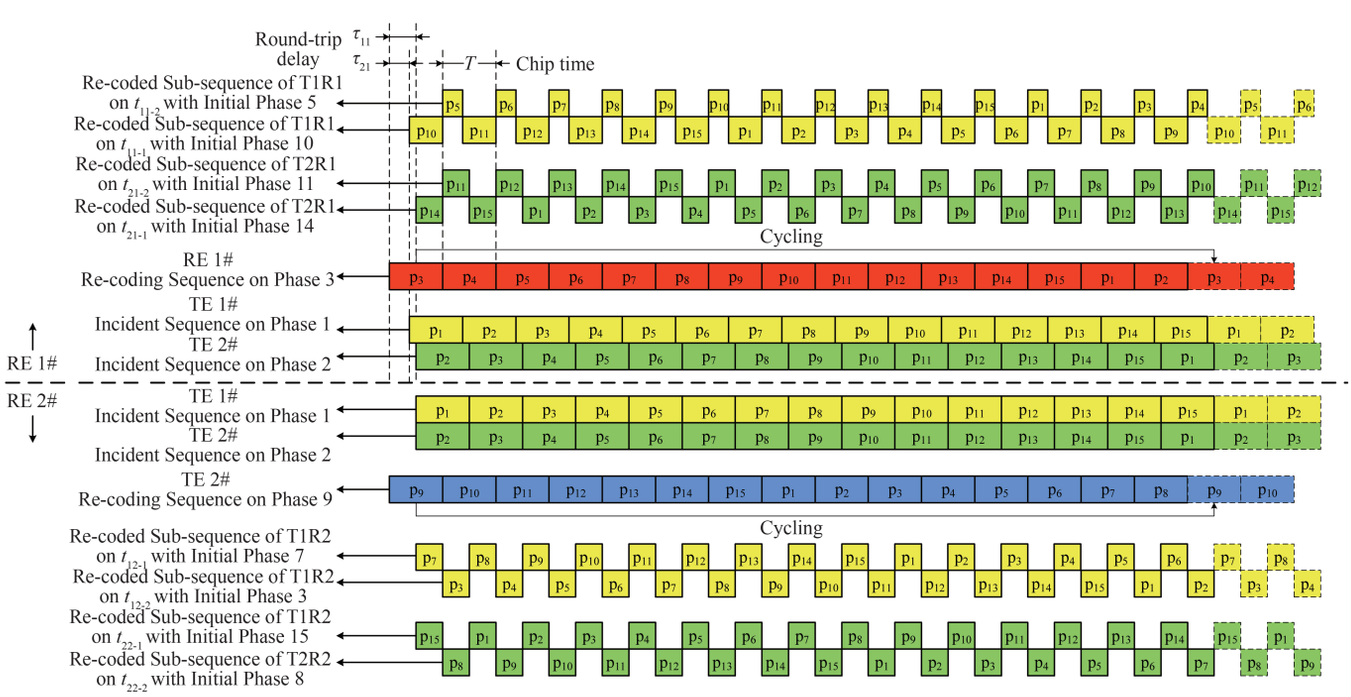

Fig. 4 The secondary CDM process of the dual-CDM in single-channel MIMO radar

图4 单通道MIMO雷达双重码分复用的二次码分复用过程

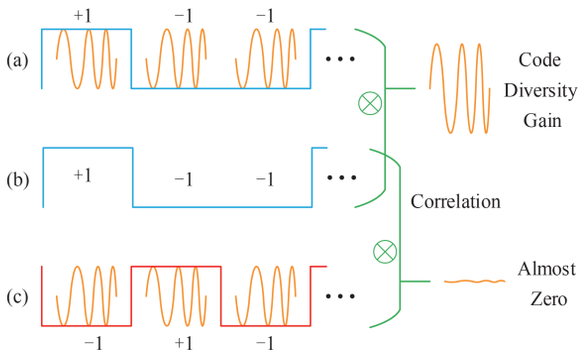

Fig. 5　Schematic diagram of two typical de-multiplex processes and their results, where the time-domain encoded signal (a) is the one to be extracted this time, (b) is the de-multiplex code sequence this time, and (c) is the one not to be extracted this time
图5　两种典型的解复用过程及其结果示意图,其中时域编码信号(a)是当前要提取的信号,(b)是当前解复用信号,(c)是当前不需提取的信号

fluential factor in the de-multiplex process. Therefore, the criterion that limit both the interference and the noise will be established for this certain application.

Let $\mathbf{p}_k = [\mathrm{p}_k(1), \mathrm{p}_k(2), \cdots, \mathrm{p}_k(L)]$, $\mathrm{p}_k(l) = \pm 1, l = 1, 2, \cdots, L$ be the k-th sequence from an L-length m-sequence family, $\mathbf{h}_k = [\mathrm{h}_k(1), \mathrm{h}_k(2), \cdots, \mathrm{h}_k(L)] \in \mathbb{R}^L$ the corresponding de-multiplex code sequence, $\mathbf{V} = [\mathbf{p}_1^{\mathrm{T}}, \mathbf{p}_2^{\mathrm{T}}, \cdots, \mathbf{p}_k^{\mathrm{T}}, \cdots, \mathbf{p}_L^{\mathrm{T}}]$ the input array consisting of all the L-length m-sequences, where $[\cdot]^{\mathrm{T}}$ denotes the transpose operator. Without loss of generality, let us assign $\mathbf{p}_k$ as the sequence to be extracted, then the correlation output is written as

$$\mathbf{y}_k = \mathbf{h}_k \mathbf{V} = [\mathrm{y}_k(1), \mathrm{y}_k(2), \cdots, \mathrm{y}_k(l), \cdots, \mathrm{y}_k(L)], \quad (1)$$

where $\mathrm{y}_k(k)$ is the amplitude gain of $\mathbf{p}_k$. Let σ^2 be the variance of the Gaussian noise, the SNR of the k-th sequence's correlation output is defined as

$$\mathrm{SNR}_{\mathbf{h}_k} = 10\log_{10}\left(\frac{\mathrm{y}_k(k)}{\left\|\mathbf{h}_k\right\|_2^2 \sigma^2}\right), \quad (2)$$

where $\|\cdot\|_2$ denotes the l-2 norm. Here we note that, the SNR in Eq. 2 is not defined by the power but the amplitude. That is because we want to provide a more specific results compared with the correlation amplitude for simplicity in the following section, and definition with the power also works here. As for the mutual interference, the signal-to-interference ratio (SIR), which describes the ratio between the output powers of the expected signal and the unexpected counterparts, is introduced as another factor to evaluate the performance. Actually, not all the sequences in this m-sequence family will be generated after the dual-CDM process. Let $\mathcal{L}$ be the set of all the m-sequences' indexes, $\mathcal{L}_1 \subset \mathcal{L}$ be the set of L_1 sequences that will be generated, and $\mathcal{L}_2 \subset \mathcal{L}$ be the set of the rest L_2 sequences, then there will be $\mathcal{L}_1 \cap \mathcal{L}_2 = \varnothing$, $\mathcal{L} = \mathcal{L}_1 + \mathcal{L}_2$ and $L = L_1 + L_2$. When extracting $\mathbf{p}_k, k \in \mathcal{L}_1$, the SIR of the k-th sequence's correlation output is defined as

$$\mathrm{SIR}_{\mathbf{h}_k} = 10\log_{10}\left(\frac{\mathrm{y}_k^2(k)}{\sum_{l \in \mathcal{L}_1, l \neq k} \mathrm{y}_k^2(l)}\right). \quad (3)$$

It can be derived from Eq. 2 that an SNR of L/σ^2 can be obtained using the same m-sequence as the de-multiplex code. However, Eq. 3 shows that the same m-sequence yields an SIR of $L^2/(L-1)$ because the correlation result of -1 in the other shift-phases [23], which results in the mutual interference by the incomplete shift-phase orthogonality. To suppress the mutual interference, the TSOC generated by setting the positive values of the m-sequences to 0 while keeping the negative values is presented as a de-multiplex code in Ref. [16]. This design results in absolute zero values on the shift-phase correlation and yields an SIR of $+\infty$. Unfortunately, the TSOC achieves an SNR of $(L+1)/2\sigma^2$, which is only about half of what m-sequence does.

Nevertheless, we note that m-sequences come in some specified lengths $2^n - 1$ [23]. If the number of sequences need to be extracted doesnot fall onto $2^n - 1$, a certain redundancy is unavoidable, providing the opportunity to re-allocate the energy in the correlation function. Specifically speaking, the total output energy of the sequences in $\mathcal{L}_1$ except for the one to be extracted should be constrained as small as possible, while the energy of the sequences in $\mathcal{L}_2$ does not matter. This re-allocation can be realized by mismatched filter (MMF) and is a potential solution for designing a better de-multiplex code.

2.2　Design method of optimized de-complex code

Based on the criterion discussed above, a novel design method of optimized de-complex code based on MMF code (MMFC) will be proposed in this section. Different from the matched filter, the proposed method is to maximize $\mathrm{SNR}_{\mathbf{h}_k}$ and $\mathrm{SIR}_{\mathbf{h}_k}$ for the extraction of $\mathbf{p}_k$ $\forall k \in \mathcal{L}_1$. However, directly optimizing both SNR and SIR at the same time results in a multi-objective optimization that is hard to solve directly. From Eqs. 2-3, it is similar in mathematics to maximize the SNR and SIR as they both need to achieve a high $\mathrm{y}_k(k)$ and suppress the total power of noise and interference. To constrain the noise, the constraint of $\left\|\mathbf{h}_k\right\|_2^2 \leqslant L^2$ can be established. As for the interference, it can be upper-bounded by $\mathrm{y}_k^2(l) \leqslant \varepsilon, l \in \mathcal{L}_1, l \neq k$, where ε is a tiny positive value. Then through maximizing the amplitude gain, the design of the MMFC for the extraction of $\mathbf{p}_k$ can be formulated into an optimization problem as

$$\begin{aligned} &\max_{\mathbf{h}_k} \mathrm{y}_k(k), l \in \mathcal{L}_1, l \neq k \\ &\text{s.t.} \left\|\mathbf{h}_k\right\|_2^2 \leqslant L^2 \\ &\mathrm{y}_k^2(l) \leqslant \varepsilon, l \in \mathcal{L}_1, l \neq k \end{aligned}. \quad (4)$$

For the optimization problem, the objective is linear and the two constraints are both convex. Therefore, the optimization problem is a convex one that can be easily solved by standard numerical tool such as CPLEX [24].

To verify the design's performance, several numerical simulations are executed on a 63-length m-sequence

family. Without loss of generality, σ^2 is set as 1, ε is set as 0.01 to achieve a 20dB suppression on the interference power, and $\mathbf{p}_1$ is assigned the one to be extracted. Fig. 5 depicts the correlation output of sequence $\mathbf{p}_1$, where 32 continuous sequences $\mathbf{p}_1$-$\mathbf{p}_{32}$ are included into $\mathcal{L}_1$.

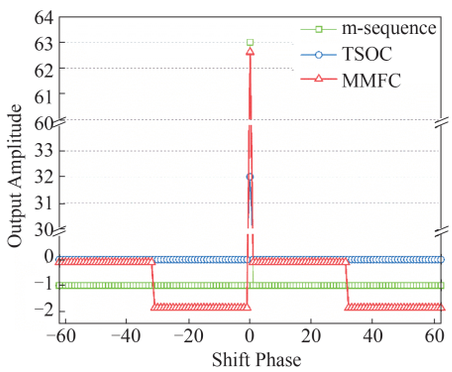

Fig. 6 Comparison of the correlation output between m-sequence, TSOC and MMFC
图6 原始m序列、完全移位正交码与失配滤波器码的相关输出比较

As shown in Fig. 6, correlation output of proposed MMFC has a 0.6% loss on amplitude gain than that of the m-sequence, but it is far better than that of the TSOC about 50%. Furthermore, MMFC introduces just 0.1 interference in amplitude compared to the root square of ε.

The SNR and SIR performances with different element number L_1 under Monte-Carlo simulations are shown in Figs. 7-8, separately. It is worth highlighting that it does not make sense to calculate the SIR for TSOC for its values identically equal to $+\infty$.

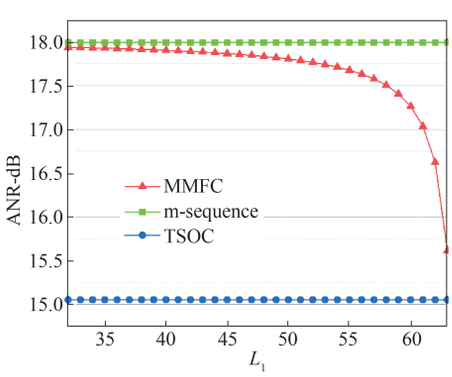

Fig. 7 Comparison of the defined SNR between m-sequence, TSOC and MMFC
图7 m序列、完全移位正交码与失配滤波器码的解复用输出信噪比

It is not surprising to see that both the SNR and SIR of MMFC become worse as L_1 increases, because the redundancy for energy re-allocation tends less. However, the proposed MMFC always keeps better SNR than that of TSOC, while it overcomes the m-sequence by its better SIR performance. The SNR of MMFC decreases within 0.5 dB compared with that of m-sequence as far as $L_1 \leqslant$ 58, while that of TSOC is almost 3dB. As for the SIR, although interferences are unavoidable using MMFC, they are much lower than that of m-sequence (about -20 dB).

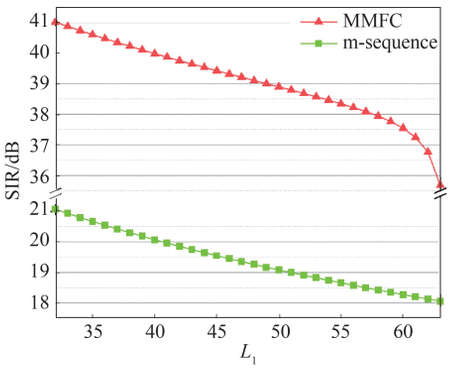

Fig. 8 Comparison of the SIR between m-sequence and MMFC
图8 m序列与失配滤波器码的解复用输出信干比

3 Simulation and experiment

To verify the correctness and validity of the proposed methods of the single-channel MIMO radar, a simulation and an experiment are executed in this section.

3.1 Simulation

To present the detail of the secondary CDM process, a simulation based on a single-channel MIMO radar whose elements are deployed as a 2 × 2 linear array and allocated with several 15-length m-sequences as Fig. 4 is performed. In this simulation, the TEs and the REs are deployed as Fig. 9 shown, with a point target set 1m away from the array. In addition, linear frequency modulation continuous wave (LFMCW) whose frequency ranging from 39GHz to 41GHz are added with white Gaussian noise of 10dB SNR and then modulated in each single chip of the m-sequences. After generating 15-cycle ideal LFMCW pulses, the 1-st and the 2-nd m-sequences are multiplied as the transmitted signals for the two TEs, respectively. Then they will be captured by two REs and re-coded by the 3-rd and the 9-th sequences, providing the mixed signals for the further de-multiplex process.

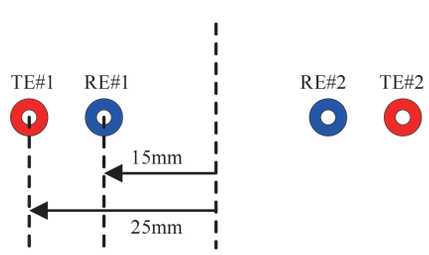

Fig. 9 The 2 × 2 liner array used for the simulation
图9 仿真所用2×2线性阵列布阵

Without loss of generality, only the echo of RE 1# is given as Fig. 10(a), whose re-coded counterpart is also shown as Fig. 10(b) with some obvious phase shifts marked. The aggregated signal is shown as Fig. 10(c). Meanwhile, the extracted results of the echoes of observation channel 1# (TE 1# and RE 1#) are presented as fol-

lows. In this channel, the 10-th and the 5-th m-sequences based MMFC should be used for de-multiplex, after which the resulted signals are shown in Figs. 10(d~e). It is obvious that the two effective outputs complement each other well on the time axis, proving the conclusion in Fig. 4. Finally, the two complementary components should be added as the complete de-multiplexed signal of observation channel 1# as Fig. 10(f).

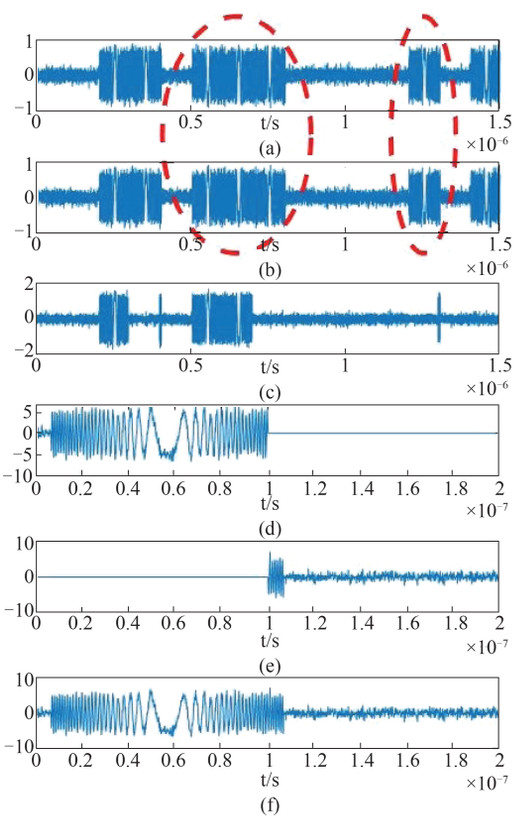

Fig. 10　The simulated signals for one exemplary observation channel during the single-channel 2 × 2 MIMO imaging, where (a) is the received signal, (b) is the re-coded signal, (c) is the aggregated signal, (d) is one of the de-multiplexed signal, (e) is the other de-multiplexed signal and (f) is the final de-multiplexed signal combined of (d) and (e)
图 10　单通道 2×2 MIMO 雷达成像过程中的一个示例观测通道信号仿真结果,其中:(a)是接收到的信号,(b) 是二次编码后的信号,(c)是聚合信号,(d)该信号的其中一个解复用信号,(e)是该信号的另一个解复用信号,(f)是(d)与(e)结合形成的该路最终解复用信号

Obtaining the four observation signals, the data is processed by back projection (BP) algorithm for imaging. The two-dimensional BP image of the scene is shown in Fig. 11, which has the quite similar performance with the traditional multi-channel MIMO radar system.

3.2　Experiment

As shown in Figs. 12(a-b), a prototype whose antennas' phases can be shifted as 0/π arbitrarily by the control of the computer is developed, while Fig. 12(c) presents the block diagram of this system.

In the prototype, a pair of transmit and receive antennas, which are both in form of pyramid horn, are separately deployed on a programmable scanning platform with two scanners. With the help of these two scanners, the transmit and the receive antennas can move horizontally and vertically, respectively, which formulate a "T" shape observation in the space. During each transmit step, a vector network analyzer (VNA) collects a series of *S*21 data between the T/R antennas from 32 ~ 38 GHz, which provides the one-dimensional high-resolution image along the distance. Limited by the number of the antennas, the multiple TEs and multiple REs are equivalently achieved by the observations at different positions. To achieve the images with satisfactory performance, a 26×26 MIMO radar is equivalently realized as shown in Fig. 13 by scanning the T/R antennas along with a 50 cm range with the step of 2 cm, respectively. Mixing the observed signals together, it can be treated as the single-

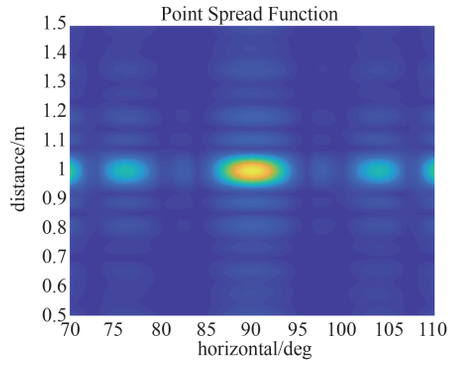

Fig. 11　The point spread function of the simulated single-channel MIMO radar in distance-horizontal dimension
图 11　所仿真单通道 MIMO 雷达在水平-距离方向的点扩展函数

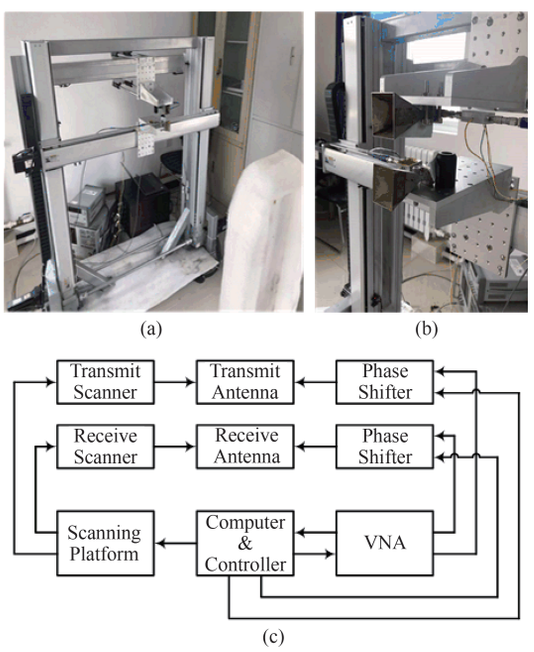

Fig. 12　Photograph of (a) the imaging system prototype and (b) the phase shifters as well as the (c) block diagram of this system
图 12　(a)成像系统(b)移相器的照片以及(c)系统原理框图

channel data for the further de-multiplex process.

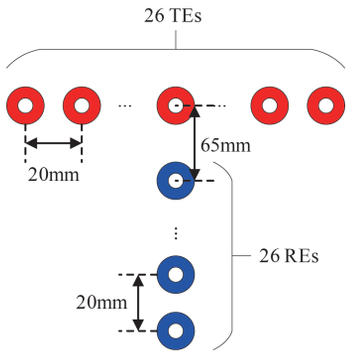

Fig. 13 The simulated 26 × 26 "T" shape MIMO array by scanning used for the experiment
图13 扫描实验模拟的26×26 "T"型MIMO阵列示意图

In the experiment, the targets such as scissors, CD and knife are fixed against a piece of plastic foam and placed approximately 1m away from the array, resulting a nearfield imaging scene that usually happens in security imaging. These targets are then imaged by the designed single-channel MIMO radar system prototype. To verify the system's performance to detect conceal targets, some of the items are covered by clothes. The demultiplex is executed using m-sequence, TSOC and MMFC as the de-multiplex code. Furthermore, the imaging is done with BP as what used in the simulation in Sect. 3.1. Photos and imaging results with a dynamic range of 10dB are shown in Figs. 14-15, respectively.

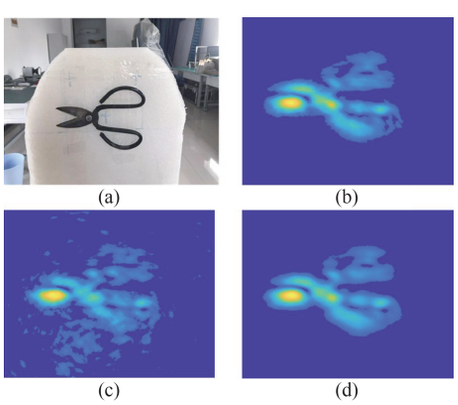

Fig. 14 (a) Photograph of the target; Single-channel MIMO radar imaging by (b) m-sequence (c) TSOC (d) MMFC
图14 (a)目标照片;利用(b)m序列(c)TSOC(d)MMFC进行的单通道MIMO雷达成像

Figure 14 shows the photograph and the imaging result of a pair of scissors. The images of m-sequence and MMFC do have a relatively higher SNR than that of the TSOC. However, the image of MMFC has a more distinct edge than that of m-sequence due to the higher SIR.

To verify the system's performance to detect conceal targets, a knife and a CD are placed under a linen T-shirt and imaged. The imaging scene, targets and imaging results are shown in Fig. 15. In the knife's image, the metal part of the knife stands out while the plastic part fades. As for the CD, its shape keeps well in image for its strong reflection character.

Fig. 15 Imaging test of the targets under clothes
图15 目标置于衣物下的成像实验

Overall, it can be seen from these experiments that the single-channel MIMO radar can achieve the similar imaging performance with the traditional multi-channel MIMO radar, providing the potential for the low-cost and low-complexity security imaging radar system.

4 Conclusion

In order to reduce the cost and complexity of the traditional multi-channel MIMO radar, the dual-CDM technique has been proposed in this paper for implementing the mmW MIMO security imaging radar system relying on a single transmit/receive channel. Firstly, the architecture and implementation method of the dual-CDM MIMO radar has been discussed, and the orthogonality of all the dual-CDM signals has been analyzed. As a step further, the optimized de-multiplex code design method has been proposed based on mismatched filter theory, which yields the maximum code-diversity gain against the noise and interference. Finally, both the simulation and the experimental results have been given to verify the correctness and validity of the proposed methods. By employing the proposed methods, the signal-channel MIMO radar can achieve a comparable performance with that of its multi-channel counterpart with far less hardware complexity.

References

[1] Kemp M C. Millimetre wave and terahertz technology for detection of concealed threats-a review[C]//2007 Joint 32nd International Conference on Infrared and Millimeter Waves and the 15th International Conference on Terahertz Electronics. IEEE, 2007: 647-648.
[2] CHENG Hang, ZHENG Hai-Tao, JING Han-Dan, *et al*. Three-dimensional near-field surveillance imaging using W-band system [J]. *Journal of Infrared and Millimeter Waves*(程航, 郑海涛, 敬汉丹, 等. W波段三维近场安检成像系统. **红外与毫米波学报**), 2017, **36**(4):408-414.
[3] Luukanen A, Appleby R, Kemp M, *et al*. *Terahertz Spectroscopy and Imaging: Millimeter-wave and terahertz imaging in security applications*[M]. Springer, Berlin, Heidelberg, 2012: 491-520.
[4] Liu T, Zhao Y, Wei Y, *et al*. Concealed object detection for activate millimeter wave image[J]. *IEEE Transactions on Industrial Electronics*, 2019, **66**(12):9909-9917.
[5] Jacobs E L. Reflect-array based mm-wave people screening system [J]. *Proceedings of SPIE - The International Society for Optical Engineering*, 2013, **8900**(6): 02.
[6] Roe K J, Gregory C W. Wave-based sensing and imaging for security applications [C]//European Conference on Antennas and Propagation, 2015: 1-5.

[7] Sheen D M, Mcmakin D L, Hall T E. Three-dimensional millimeter-wave imaging for concealed weapon detection[J]. *IEEE Transactions on Microwave Theory & Techniques*, 2001, **49**(9): 1581-1592.
[8] Ahmed S S, Schiessl A, Gumbmann F, *et al*. Advanced microwave imaging[J]. *IEEE microwave magazine*, 2012, **13**(6): 26-43.
[9] Mcmillan R W, Currie N C, Ferris D D, Jr, *et al*. Concealed weapon detection using microwave and millimeter wave sensors[C]//International Conference on Microwave and Millimeter Wave Technology Proceedings, 1998: 1-4.
[10] Kocamış M B. Optimal design of sparse mimo arrays for wideband near-field imaging based on a statistical framework[D]. , 2018.
[11] Chen Q, Tong N, Li X, *et al*. Sparse MIMO planar array two-dimensional imaging based on IF-MMV-SBL algorithm [J]. *Journal of Physics: Conference Series. IOP Publishing*, 2019, **1314** (1): 012193.
[12] Donoho D L. Compressed sensing [J]. *IEEE Transactions on Information Theory*, 2006, **52**(4): 1289-1306.
[13] Zhao X, Yang Q, Zhang Y. Compressed sensing approach for pattern synthesis of maximally sparse non-uniform linear array[J]. *IET Microwaves, Antennas & Propagation*, 2013, **8**(5): 301-307.
[14] Gumbmann F, Schmidt L P. Millimeter-wave imaging with optimized sparse periodic array for short-range applications[J]. *IEEE Transactions on Geoscience & Remote Sensing*, 2011, **49**(10): 3629-3638.
[15] Lynch J J. Low latency digital beamforming radar using aperture coding [J]. *IEEE Transactions on Aerospace and Electronic Systems*, 2016, **52**(2): 918-927.
[16] Bergamo M A. Spread spectrum digital beamforming (SSDBF) radar [C]//2010 IEEE International Symposium on Phased Array Systems and Technology. IEEE, 2010: 665-672.
[17] Mondal D, Basak S, Bera R, *et al*. Integrated hybrid DBF vehicular radar[J]. International Journal of Engineering and Advanced Technology, 2014, **3**(3): 61-70.
[18] Bera S, Sur S N, Bera R. Spread spectrum-digital beam forming radar with single RF channel for automotive application[C]//9th International Radar symposium. 2013: 1-5.
[19] Shome S, Bera R N, Sur S N, *et al*. Moving target detection and Doppler extraction using digital spread spectrum radar[J]. *International Journal of Intelligent Systems and Applications*, 2014, **6**(10): 47.
[20] LOU Bao-Fang , LIU Zhi-Guo. A new low-cost technology on phased array radar[J]. *Radar Science and Technology*(娄宝芳, 刘志国. 一种高性价比的相控阵雷达新技术. **雷达科学与技术**), 2015, **13**(03):27-30.
[21] LOU Bao-Fang. Research on antenna reconfigured software defined radar architecture[J]. *Modern Navigation*(娄宝芳. 一种天线配置软件定义雷达架构研究. **现代导航**), 2018, **9**(05):44-48.
[22] Han S, Chih-Lin I, Xu Z, *et al*. Large-scale antenna systems with hybrid analog and digital beamforming for millimeter wave 5G[J]. *IEEE Communications Magazine*, 2015, **53**(1): 186-194.
[23] XU Min. The shift-and-add property of m-sequence[J]. *Journal of Mathematics in Practice and Theor*(徐敏. *m*序列的移位相加性. **数学的实践与认识**), 1995, **1**:63-64.
[24] IBM: CPLEX Optimizer[OL]. 2018. https://www.ibm.com/analytics/cplexoptimizer.